Exploring the Formation of Symmetric Gold Nanostars by Liquid-Cell Transmission Electron Microscopy

Nabeel Ahmad, Guillaume Wang, Jaysen Nelayah, Christian Ricolleau, Damien Alloyeau

Exploring the Formation of Symmetric Gold Nanostars by Liquid-Cell Transmission Electron Microscopy

Nabeel Ahmad,[1,2] Guillaume Wang,[1] Jaysen Nelayah,[1] Christian Ricolleau,[1] and Damien Alloyeau[1,]*

1. Laboratoire Matériaux et Phénomènes Quantiques UMR 7162, Université Paris Diderot, Sorbonne Paris Cité, CNRS, 75013, Paris, France

2. School of Chemical and Materials Engineering (SCME), National University of Sciences and Technology (NUST), H-12, Islamabad, Pakistan

ABSTRACT.

The shape-dependent properties of gold nanostars (NSs) have motivated massive research efforts in the field of colloidal chemistry to gain a better control over the morphology of these promising nanostructures. Nevertheless, this challenge requires a better understanding of the atomic-scale processes leading to the formation of stellated nanoparticles. We hereby report an unprecedented *in situ* study focused on the seed-mediated synthesis of symmetric gold nanostars (NSs) performed by radiolysis in methanol. We take advantage of the spatial and temporal resolutions of liquid-cell transmission electron microscopy (LCTEM) to unravel the key effects of the growth speed, seed-crystal morphology and dimethylamine functionalization on the formation mechanisms, shape and stability of NSs enclosed by high-index facets. Surprisingly, the stellation processes transforming icosahedral nanoparticles into NSs with 20 sharp arms entails a continuous restructuring of NS facets driven by surface diffusion, which provide a fresh look at faceting mechanisms.

KEYWORDS: symmetric gold nanostars, seed-mediated synthesis, dimethylamine functionalization, growth processes, stellation, liquid-cell TEM.

The last two decades have witnessed a remarkable increase in research activities related to the synthesis and characterization of gold nanocrystals. This increased interest can be attributed to the promising size and shape dependent physicochemical properties of Au nanoparticles, which can be exploited for various interdisciplinary research areas including but not limited to plasmonics, biomedicine and catalysis just to name a few.[1-5] Although Au nanoparticles with very various shapes has been fabricated, recent attention has shifted towards the synthesis of Au nanostars (NSs), as these multi-branched nanostructures with a central core, provide an opportunity to expand the broadening horizon of applications of gold nano-objects.[6] The distinguishing feature of Au NSs over other morphologies is the presence of arms with sharp tips that give rise to narrow and tuneable surface plasmon resonance (SPR) throughout the entire visible and near IR spectrum holding much promise for biomedical applications.[7-9] Also, the local field strength near the apexes of the arms is enhanced significantly compared to incident light thus making a strong case for exploiting surface enhanced Raman spectroscopy (SERS) applications.[10-13] Although some one-pot methods have been reported, most wet-chemical syntheses of Au NSs combine both seed and functionalization-mediated growth.[14, 15] All these protocols involved the reduction of chloroauric acid ($HAuCl_4$) by strong or mild reducing agent (ascorbic acid, Dimethylformamide, HEPES, hydrazine…) in presence of one or several capping agents (CTAB, CTAC, PVP, citrate…) to induce anisotropic growth of branches on preformed seed. Although these NSs have been studied for various applications, it remains challenging to exploit the full potential of these nano-objects because of their random shape. Indeed, the variation in the number and length of branches together with the

rounded shape of the tips has detrimental effect on the optical properties of the Au NSs.[16] The poor control over NS symmetry raises awareness about the need to understand the atomic-scale mechanisms driving nanocrystal shape. The sophistication of nanostructure morphology and the complexity of experimental protocols combining several strategies to control the shape of nanomaterials make this task inherently difficult and favor the use of empirical approaches to improve bottom-up synthesis methods. Liquid-cell transmission electron microscopy (LCTEM) has opened up a new way to overcome this critical issue of nanomaterials synthesis by making possible *in situ* observation of nanocrystal formation in controlled-liquid environment.[17-19] For a few years, this MEMS-based TEM technique has allowed studying both kinetic and thermodynamic effects on the growth of nanomaterials that are dictated by the flows of matter and the stability of nanomaterials within their formation medium, respectively.[20-22] Therefore, many strategies to control the shape of nanomaterials have been studied *in situ*, including the seed-mediated[23, 24] and the face-blocking methods.[25] In this paper, we have performed TEM imaging in methanol to reveal the effects of growth speed, seed structure and alkylamine functionalization on the formation processes and stabilization of NSs enclosed by high-index facets. This work provides valuable *in situ* insights on the synthesis of symmetric NSs with tunable and controlled shape in a simple alcohol solvent.

Like large-scale syntheses, the fabrication of gold NSs within the liquid-cell is based on two-step approach, consisting in the formation of seeds and the subsequent growth of NSs (see experimental details and figure S1 in supplementary information). Seed crystals were grown radiolytically in several areas of the liquid cell in a solution that contain only gold precursors ($HAuCl_4$) in methanol. The radiolysis of this polar solvent presents many similarities with the radiolysis of water,[26, 27] notably the production of solvated electrons (e_s^-) that are primarily responsible for the reduction

of gold ions to gold monomers which cluster together to form nanoparticles. As in water,[21, 22] the morphology of the nanostructures synthesized in methanol depends on the electron dose rate ($\dot{d}$) and low $\dot{d}$ regime (< 10^{-2} electrons/sÅ^2) favours the formation of highly faceted seeds. The beam-driven growth is then dominated by thermodynamic effects because the low adsorption rate of gold atoms on surface provides enough time for nanoparticles to reach energetically-stable shapes, corresponding to local minima in the Gibbs free energy of formation that are known to vary with temperature and nanoparticle size.[28] As shown in figure 1, three types of nanocrystals are mainly formed under such conditions: 2D plates and 3D icosahedral and decahedral particles. The shape of the 3D nanostructures can be ambiguous on low-magnification images acquired in liquid due to poor resolution and the misorientation of the nanocrystals with respect to their main symmetry axes. Nevertheless, high resolution imaging (HRTEM) performed *ex situ* after this seed-growth step, clearly revealed that 2D plates, icosahedral and decahedral particles are formed, with proportions of 21.8%, 38.7% and 13.8 %, respectively. For example, the projected shapes and the characteristic atomic contrasts observed in figures 1c and 1d allow identifying an icosahedral and a decahedral nanoparticle along their three-fold and five-fold rotational-symmetry axes, respectively.[24, 29, 30] While the Au platelets have a large size dispersion, icosahedral and decahedral particles have a mean size of 33 ± 9 nm and 51 ± 11 nm, respectively. Other morphologies such as bi-pyramids and nanorods can also be sparsely found (Fig. S2).

The diversity in nanocrystal shapes is dictated by the formation of planar defects that break the cubic symmetry of the gold atomic lattice. As illustrated in Figure S2c, we systematically observed 1/3 422 reflections on the Fourier transform of the HRTEM images of 2D nanoplates. The presence of this theoretically forbidden reflections arises from the stacking of planar defects (stacking faults or twin planes) all parallel to the top and bottom (111) faces.[31-33] As previously reported, this

peculiar configuration of crystal defects creates preferential adsorption sites on the side face of the nanostructures and promotes their 2D growth along the (111) plane.[34-36] On the contrary, the growth of facetted 3D nanoparticles arises from multiple twinning processes along different directions. Interestingly, the two large facets of the 2D plates, the 20 triangular facets of the icosahedral particles and the 10 triangular facets of decahedral particles are all (111) planes, which are known to be stable because of their low surface energy. The low magnification used to form these facetted nanostructures does not allow studying dynamical twining processes to distinguish, for example, if 3D multi-twined particles are formed through nucleation-based layer-by-layer growth or successive growth twinning.[37] In the following, icosahedral nanoparticles are used as seeds for the formation of 3D NSs.

The seed-mediated synthesis of Au NS was carried out with the assistance of dimethylamine (DMA), because alkyl-amines have recently been identified as an efficient stabilizing agent of high-index facets leading to the formation of symmetric NSs.[16] After forming seeds in several areas of the top SiN membrane, the beam was shut off and DMA was continuously injected in the liquid cell together with gold precursors. After a homogenization time of 30 minutes, scanning mode imaging with a high angle annular dark field detector (STEM-HAADF) was used to activate and monitor the growth of NSs. Much higher magnifications were used for this second step to clearly reveal the formation processes. Figure 2a shows a series of STEM-HAADF images depicting the transformation of an icosahedral nanocrystal into a symmetric NS under a constant $\dot{d}$ of 3.4 electrons/Å^{2}s. Apart from a rounded protuberance, the projected NS displays 10 sharp arms that are uniformly distributed over the seed. As described in figure 2b, the transformation mechanisms involve the growth of a pyramidal arm on each of the 20 triangular facets of the icosahedral seeds. These first *in situ* insights on NS formation confirm the stellation processes deduced from both

theoretical and *ex-situ* investigations.[16, 38] Although it is challenging to unambiguously determine the faceting of the arms on *in situ* images, we considered that each of the triangular facet of icosahedron is split into six equal facets and the centre is then pulled outward in the form of hexagonal pyramid to give rise to NSs with 20 arms. This hexagonal symmetry is assumed according to the works of Niu *et al* in which DMA was also used to transform icosahedral nanoparticles into NSs.[16] The projection of this 3D structures along its 5-fold rotational axis corresponds to a star with 10 arms equidistant from each other that perfectly match the shape observed on STEM-HAADF images. *In situ* observations also reveal that seeds with rough faceting systematically lead to irregular NSs with missing or disoriented arms where seed surface is deformed (Fig. S3). In line with the concept of seed-mediated synthesis,[39] these results confirm that NSs derive their excellent symmetry from the faceted morphology of the icosahedral seeds. These 20 arms NSs were also observed along other rotational axis (Fig. S4) but none of them provides a clear view of the growth process because of the proximity and overlapping of the projected arms. Interestingly, decahedral seeds follow a very different growth path, since they maintain their pentagonal shape rather than transforming into stellated nanostructures (Fig. S5). Given the structural differences between icosahedral and decahedral seeds,[40, 41] the influence of strain and twinned planes could possibly be a starting point of theoretical investigations to understand these different behaviours.

The formation of hexagonal pyramids on the top of (111) facets leads towards growth of high index facets that are normally unstable.[42] Through the entire process, alkylamines play a crucial role in modifying the surface energies of the nanostructures, hence impacting their final shapes. To quantify the effect of DMA on the growth of gold NSs, we compared LCTEM experiments performed with similar $\dot{d}$, but with DMA concentrations of 0.06 mM, 0.03 mM and without DMA.

At first, DMA concentration drastically affects the growth speed of the NSs. As observed in figure 3d, the average growth rate of 0.83 nm/s measured without DMA is reduced by two and by eight by adding 0.03 and 0.06 mM of DMA in the reaction media, respectively. Note that these three experiments were performed on icosahedral seeds of same size. The initial size difference between the NSs at various DMA concentrations is due to the fact that significant DMA-dependent growth of the seeds had already taken place by the time the first image of the series was taken. Besides reducing the adsorption rate of gold atoms, DMA functionalization has a profound impact on the NS shape (Fig. 3a-c). In particular, the tip sharpness is very sensitive to DMA concentration. This crucial feature of NS shape depends on the size of the central core (D) and the length of the arms (L) that both increases during the growth of the nanostructure. Indeed, the higher the L/D ratio, the sharper the tips. The evolution of L as a function of D observed in figure 3e reveals that DMA slow-downs much more the growth of the core than the expansion of the arms, leading to shaper and smaller NSs. Furthermore, DMA also improves shape uniformity since the relative dispersion of arm lengths is halved when DMA concentration is doubled. These *in situ* analyses also reveal that in all synthesis conditions, the L/D ratio (i.e. the nanostar sharpness) reaches a maximum and then slightly decreases in subsequent growth periods (Fig. S6a), highlighting a size effect on the ability of DMA to favor the expansion of the arms with respect to the growth of the core. Although these results clearly demonstrate the role of DMA in stabilizing sharp NSs, the formation of large NSs with very short arms in absence of DMA in the liquid-cell remains unexpected. Indeed, according to Niu et al.,[16] without alkylamines icosahedral nanoparticles should transform into dodecahedral particles. With its orthogonal projection centered on a pentagonal facet, the projected shape of an octahedron has a 5 fold symmetry that is rather similar to the projected shape of a NSs with very short arms (Fig. S6b). Nevertheless, NSs obtained without any DMA have a convexity (i.e. convex hull perimeter divided by the actual perimeter) 12 % lower than the one expected for

regular dodecahedron, on account of the presence of arms creating concave surface sections (Fig. S6c). We assume that the formation of these arms is due to the presence of traces of DMA within the liquid cell. Indeed, this secondary amine is usually produced by reaction of ammonia and methanol. Thus, during our experiments, methanol could possibly react with amine groups present on the SiN windows or with traces of ammonia since this chemical product is used during the fabrication process of the liquid-cell.

High index facets are essentially low coordinated surfaces with a high density of kinks, steps and edges.[42] Such surface structures are desired traits for catalytic applications because they provide highly reactive sites.[43] However it also makes the long-term stabilisation of gold NSs challenging because of their poor stability. Besides revealing the growth process of nanomaterials, LCTEM also provides the unique opportunity to know the full fate of nanostructures in their formation media. We observed that shutting down the electron beam for a few minutes results in a complete reshaping of the NSs due to the surface diffusion of gold atoms from the tips to the concave surfaces (Fig. 4a). This common diffusion process is also observed during sintering phenomena[44] in which the migration of atoms is driven by the differences in chemical potential of surfaces with varying degree of curvatures.[39] By shutting down the electron beam we effectively cut off the supply of Au monomers to the growing NSs and also change the pH of the solution. The reshaping process is then driven by the need to reduce the overall surface energy *via* the reduction of surface area. It also highlights the inability of DMA to prevent surface atom diffusion when low-concentrations of capping agent are used. Note that this transition regime in which DMA drives the formation of NSs but cannot maintain their shape when the growth stops could not revealed by analysing *ex situ* snapshots of the nanomaterials extracted from their formation medium at given time points of the synthesis. Interestingly, increasing the DMA concentration prolongs the reshaping time and can

even ensure the long term stability of NSs when the concentration reach 0.2 mM (Figures 4b and S7). In line with the established stabilizing role of capping agent,[39] these *in situ* observations perfectly illustrate the direct link between the surface-energy equilibrium of Au NSs and the amount of capping agents on their surface. Increasing DMA concentration in the liquid-cell has also the practical advantage that the formation of NSs can be monitor with much higher magnification. Indeed, as the growth speed increases with $\dot{d}$ (Fig. S8a),[21] increasing the magnification of STEM imaging leads to growth processes dominated by kinetic effects in which the nanoparticles cannot reach well-facetted morphology and tends to rapidly coalesce because of the very high flow of adsorbed monomers (Fig. S8c). By reinforcing the stability of Au NSs and reducing the adsorption rate of gold atoms, DMA allows studying the morphology of isolated NSs with magnification up to 1 500 k (Fig. S8c).

Finally, we want to shed light on a peculiar feature of NS formation which could not be emphasised without dynamical *in situ* imaging. The habit of a crystal is determined by the relative rates at which different crystal planes grow. Thus, the faster growing facets (i.e. the more attractive for ad-atoms) are usually eliminated at the expense of slow growing ones.[39] This faceting process is well exemplified by the transformation of a 2D nanoprisms into a 2D hexagonal nanoplate observed in pure methanol (Fig. 5a). The initial nanoprisms always exhibit three (422) edges but the reshaping of the nanoprism corners lead to the formation of six (220) edges. Thereafter, Au monomers attach preferentially to the (422) edges that grow rapidly out of existence leading to hexagonal nanoplates terminated with (220) edges. Interestingly, the transformation of gold nanoprisms in water systematically follow a different pathway ending with hexagonal nanoplates with 6 (422) edges (Fig. S9). Note that the edge indexes were deduced from *ex situ* HRTEM experiments described in figures S2c, but they do not correspond to the indexes of the side-faces which are usually a mix of

(111) and (100) planes dictated by the planar-defect configuration .[31, 33, 45] In fact, as the growth rate of the nanoplate edges depends on the side-face structure,[45, 46] monitoring the growth processes in cross-section view would provide a deeper understanding of these faceting mechanisms and the impacts of solvents.

According to this very common view of crystal growth, the shape of NSs should depend on the competition between the growth of a given high-index facet, with (hkl) that would depend on DMA concentration and the growth of the (111) facets of the icosahedral seed. Therefore, NSs with apexes truncated by (111) planes should be observed during the transformation of an icosahedral seed into a NSs enclosed by high-index facets. Surprisingly, nanoscale *in situ* imaging reveals that NSs display sharp tips through the whole growth process of their arms and the expected truncation of these arms is never observed. In fact, the growth of the pyramidal arms on each triangular facet of the seeds goes through a continuous increase of the distance between the apex and the base of the pyramids (Figures 5b and associated video file). This stellation process systematically observed in all growth conditions, implies that the indexes of NS facets continuously changes during the formation of the arms, as it is evidenced by the continuous reduction of the mean inter-arms angle during NS growth (Fig. 5b). Given the dispersion of inter-arm angles that is always experimentally observed and the resemblance of NSs enclosed by facets with close (hkl) indexes, it is difficult to unambiguously determine the crystal planes at the NS surface by comparing electron microscopy images with theoretical NS shapes.[16] Like the tip sharpness, the final indexes of the facets enclosing a NSs will depend on the growth time and on the competition between the expansion of the arms and the growth of the NS core which induces a widening of the triangular base of the arms. This fresh look at the formation of nanostructures with high-index facets indicates that DMA likely enhances the surface diffusion and the mobility of kinks, steps and edges that are necessary to

continuously change crystal facets. We hope this first insights will motivate further experimental and theoretical investigations on this keystone process of NS growth.

We have exploited liquid-cell TEM to explore the growth mechanisms of gold NSs in methanol. These *in situ* investigations reveal that the symmetry of the NSs is directly related to the faceting of the initial seeds. We observed the formation of highly symmetric NSs *via* the growth of pyramidal arms on the 20 facets of icosahedral seeds. Besides confirming the efficiency of DMA to stabilise sharp NSs terminated by high-index facets, we show that the shape of NSs is driven by the competitive growth of the core and the arms of the stellated nanostructures. Interestingly, the expansion of the arms involves a continuous and very dynamic restructuring of crystal surfaces which emphasise the crucial role of DMA in the surface diffusion processes leading to the formation of high-index facets. More generally, this work shed light on the unique potential of LCTEM to study sophisticated synthesis protocols, combining both seed and functionalization-mediated strategies.

Supporting Information. Experimental details, additional figures and a video file of NS growth (accelerated 32 times) from which figure 5b was extracted. This material is available free of charge via the Internet at http://pubs.acs.org.

Corresponding Author

* Telephone : +33 1 57 27 69 83; e-mail: damien.alloyeau@univ-paris-diderot.fr

Acknowledgments

The authors declare no competing financial interest.

We gratefully acknowledge the financial support of the Region Ile-de-France (convention SESAME E1845 for the JEOL ARM 200F electron microscope installed at the Paris Diderot University), the Labex SEAM (Plas-Mag project), the CNRS (Defi-Nano Program) and National University of Sciences and Technology (NUST) for supporting the PhD grant of Nabeel Ahmad.

References

1. Grzelczak, M.; Perez-Juste, J.; Mulvaney, P.; Liz-Marzan, L. M. *Chem. Soc. Rev.* **2008,** 37, 1783-1791.
2. Sau, T. K.; Murphy, C. J. *J. Am. Chem. Soc.* **2004,** 126, 8648-8649.
3. Daniel, M.-C.; Astruc, D. *Chem. Rev.* **2004,** 104, 293-346.
4. Eustis, S.; El-Sayed, M. A. *Chem. Soc. Rev.* **2006,** 35, 209-217.
5. Li, N.; Zhao, P.; Astruc, D. *Angew. Chem., Int. Ed.* **2014,** 53, 1756-1789.
6. Chirico, G.; Borzenkov, M.; Pallavicini, P., *Gold Nanostars: Synthesis, Properties and Biomedical Application*. Springer: 2015.
7. Nehl, C. L.; Liao, H.; Hafner, J. H. *Nano Lett.* **2006,** 6, 683-688.
8. Liu, Y.; Yuan, H.; Fales, A.; Register, J.; Vo-Dinh, T. *Front. Chem.* **2015,** 3.
9. Rodríguez-Lorenzo, L.; de la Rica, R.; Álvarez-Puebla, R. A.; Liz-Marzán, L. M.; Stevens, M. M. *Nat. Mater.* **2012,** 11, 604-607.
10. Rodríguez-Lorenzo, L.; Álvarez-Puebla, R. A.; Pastoriza-Santos, I.; Mazzucco, S.; Stéphan, O.; Kociak, M.; Liz-Marzán, L. M.; García de Abajo, F. J. *J. Am. Chem. Soc.* **2009,** 131, 4616-4618.
11. Hrelescu, C.; Sau, T. K.; Rogach, A. L.; Jäckel, F.; Laurent, G.; Douillard, L.; Charra, F. *Nano Lett.* **2011,** 11, 402-407.
12. Li, M.; Kang, J. W.; Dasari, R. R.; Barman, I. *Angew. Chem.* **2014,** 126, 14339-14343.
13. Schütz, M.; Steinigeweg, D.; Salehi, M.; Kömpe, K.; Schlücker, S. *Chem. Commun.* **2011,** 47, 4216-4218.
14. Guerrero-Martínez, A.; Barbosa, S.; Pastoriza-Santos, I.; Liz-Marzán, L. M. *Curr. Opin. Colloid Interface Sci.* **2011,** 16, 118-127.
15. Pallavicini, P.; Cabrini, E.; Borzenkov, M., Gold Nanostar Synthesis and Functionalization with Organic Molecules. In *Gold Nanostars*, Springer: 2015; pp 1-23.
16. Niu, W.; Chua, Y. A. A.; Zhang, W.; Huang, H.; Lu, X. *J. Am. Chem. Soc.* **2015,** 137, 10460-10463.
17. Williamson, M. J.; Tromp, R. M.; Vereecken, P. M.; Hull, R.; Ross, F. M. *Nat. Mater.* **2003,** 2.
18. Liao, H. G.; Niu, K. Y.; Zheng, H. M. *Chem. Commun.* **2013,** 49, 11720-11727.
19. Ngo, T.; Yang, H. *J. Phys. Chem. Lett.* **2015,** 6.
20. Ahmad, N.; Le Bouar, Y.; Ricolleau, C.; Alloyeau, D. *Adv. Struct. Chem. Im.* **2016,** 2, 9.
21. Alloyeau, D.; Dachraoui, W.; Javed, Y.; Belkahla, H.; Wang, G.; Lecoq, H.; Ammar, S.; Ersen, O.; Wisnet, A.; Gazeau, F.; Ricolleau, C. *Nano Lett.* **2015,** 15, 2574-2581.
22. Woehl, T. J.; Evans, J. E.; Arslan, I.; Ristenpart, W. D.; Browning, N. D. *Acs Nano* **2012,** 6, 8599-8610.

23. Jungjohann, K. L.; Bliznakov, S.; Sutter, P. W.; Stach, E. A.; Sutter, E. A. *Nano Lett.* **2013,** 13, 2964-2970.
24. Wu, J.; Gao, W.; Wen, J.; Miller, D. J.; Lu, P.; Zuo, J.-M.; Yang, H. *Nano Lett.* **2015,** 15, 2711-2715.
25. Liao, H.-G.; Zherebetskyy, D.; Xin, H.; Czarnik, C.; Ercius, P.; Elmlund, H.; Pan, M.; Wang, L.-W.; Zheng, H. *Science* **2014,** 345, 916-919.
26. Baxendale, J. H.; Wardman, P., *The Radiolysis of Methanol: Product Yields, Rate Constants, and Spectroscopic Parameters of Intermediates*. National Bureau of Standards: 1975.
27. Ferradini, C.; Jay-Gerin, J. P. *Radiation Physics and Chemistry* **1996,** 48, 473-480.
28. Barnard, A. S.; Young, N. P.; Kirkland, A. I.; van Huis, M. A.; Xu, H. *Acs Nano* **2009,** 3, 1431-1436.
29. Ling, T.; Xie, L.; Zhu, J.; Yu, H.; Ye, H.; Yu, R.; Cheng, Z.; Liu, L.; Liu, L.; Yang, G.; Cheng, Z.; Wang, Y.; Ma, X. *Nano Lett.* **2009,** 9, 1572-1576.
30. Zhang, Q.; Xie, J.; Yang, J.; Lee, J. Y. *Acs Nano* **2009,** 3, 139-148.
31. Germain, V.; Li, J.; Ingert, D.; Wang, Z. L.; Pileni, M. P. *J. Phys. Chem. B* **2003,** 107, 8717-8720.
32. Kirkland, A. I.; Jefferson, D. A.; Duff, D. G.; Edwards, P. P.; Gameson, I.; Johnson, B. F. G.; Smith, D. J. *Proc. R. Soc. London Ser. A-Math. Phys. Eng. Sci.* **1993,** 440, 589-609.
33. Le Beulze, A.; Duguet, E.; Mornet, S.; Majimel, J.; Treguer-Delapierre, M.; Ravaine, S.; Florea, I.; Ersen, O. *Langmuir* **2014,** 30, 1424-1434.
34. Berriman, R. W.; Herz, R. H. *Nature* **1957,** 180, 293-294.
35. Goessens, C.; Schryvers, D.; Vanlanduyt, J.; Amelinckx, S.; Verbeeck, A.; Dekeyzer, R. *J. Cryst. Growth* **1991,** 110, 930-941.
36. Lofton, C.; Sigmund, W. *Adv. Funct. Mater.* **2005,** 15, 1197-1208.
37. Liao, H.-G.; Shao, Y.; Wang, C.; Lin, Y.; Jiang, Y.-X.; Sun, S.-G. *Mater. Lett.* **2014,** 116, 299-303.
38. Burt, J. L.; Elechiguerra, J. L.; Reyes-Gasga, J.; Martin Montejano-Carrizales, J.; Jose-Yacaman, M. *J. Cryst. Growth* **2005,** 285, 681-691.
39. Xia, Y. N.; Xiong, Y. J.; Lim, B.; Skrabalak, S. E. *Angew. Chem.-Int. Edit.* **2009,** 48, 60-103.
40. Hofmeister, H., Shape variations and anisotropic growth of multiply twinned nanoparticles. In *Zeitschrift für Kristallographie International journal for structural, physical, and chemical aspects of crystalline materials*, 2009; Vol. 224, p 528.
41. Patala, S.; Marks, L. D.; Olvera de la Cruz, M. *J. Phys. Chem. C* **2013,** 117, 1485-1494.
42. Quan, Z.; Wang, Y.; Fang, J. *Acc. Chem. Res.* **2013,** 46, 191-202.
43. Zhou, Z.-Y.; Tian, N.; Li, J.-T.; Broadwell, I.; Sun, S.-G. *Chem. Soc. Rev.* **2011,** 40, 4167-4185.
44. Alloyeau, D., Transmission Electron Microscopy: A Multifunctional Tool for the Atomic-scale Characterization of Nanoalloys. In *Nanoalloys: synthesis, structure and properties*, Alloyeau, D.; Mottet, C.; Ricolleau, C., Eds. Springer London: 2012; pp 113 - 157.
45. Bogels, G.; Meekes, H.; Bennema, P.; Bollen, D. *J. Cryst. Growth* **1998,** 191, 446-454.
46. Bogels, G.; Pot, T. M.; Meekes, H.; Bennema, P.; Bollen, D. *Acta Crystallogr. Sect. A* **1997,** 53, 84-94.

Figures

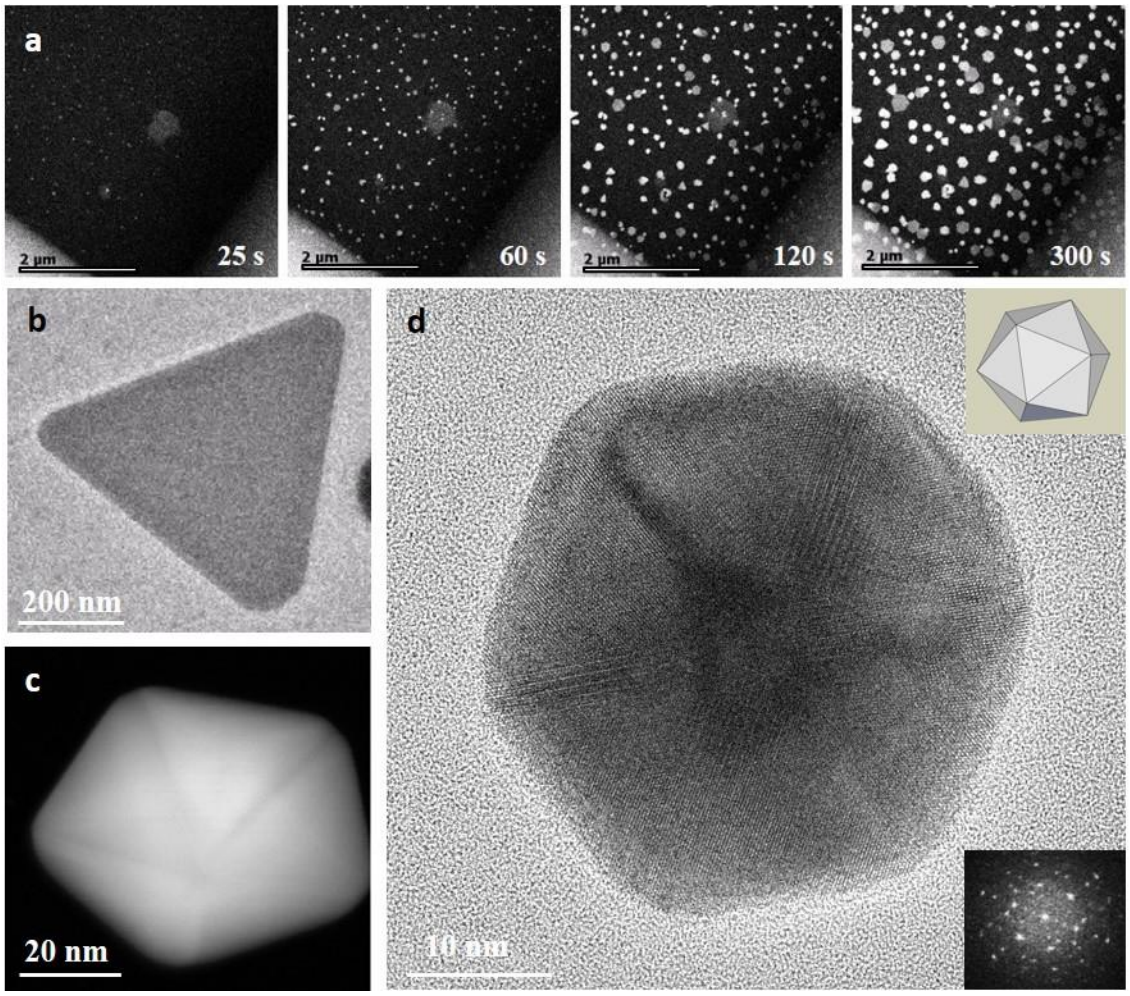

Figure 1. Nucleation and growth of Au seeds in methanol (a) Time series of STEM-HAADF image series acquired with $\dot{d} = 4.1 \times 10^{-3}$ electrons/Å^{2}s in the corner of the liquid-cell showing the nucleation and growth of 2D and 3D nanostructures in methanol. The irradiation time of the observed area is indicated in the bottom right corner of each image **(b)** *Ex situ* TEM image of a nanoprism formed in the liquid-cell. **(c)** *Ex situ* STEM-HAADF image of a decahedral particle with its (111) triangular facet parallel to the substrate. **(d)** *Ex situ* HRTEM of an icosahedral particle along the three fold rotational axis. The FFT of the HRTEM image and a 3D model of the icosahedral particle are in the bottom and top right inserts, respectively. Such icosahedral particles served as seeds for the formation of symmetric NSs.

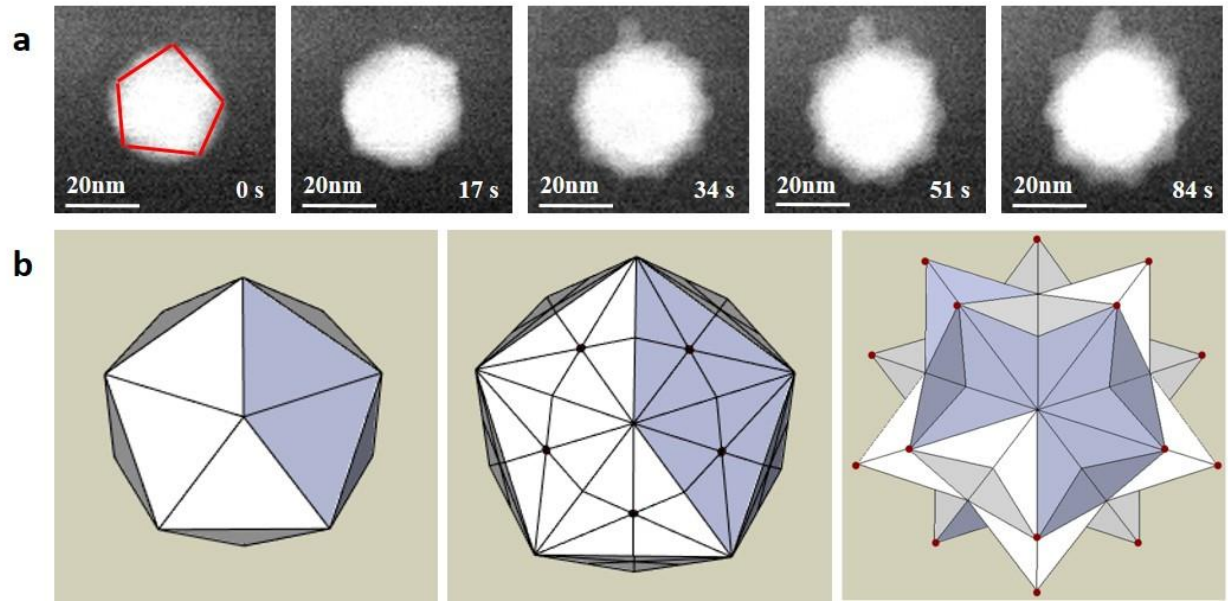

Figure 2. DMA-assisted transformation of an icosahedral seeds into a symmetric NS. (a) Time series of STEM-HAADF images acquired in methanol with DMA concentration of 0.06 mM and $\dot{d}$ = 3.4 electrons/Å^{2}s The irradiation time of the observed area is indicated in the bottom right corner of each image **(b)** Geometric model elucidating the transformation process *via* the growth of hexagonal pyramids on each triangular facet of the icosahedral seed.

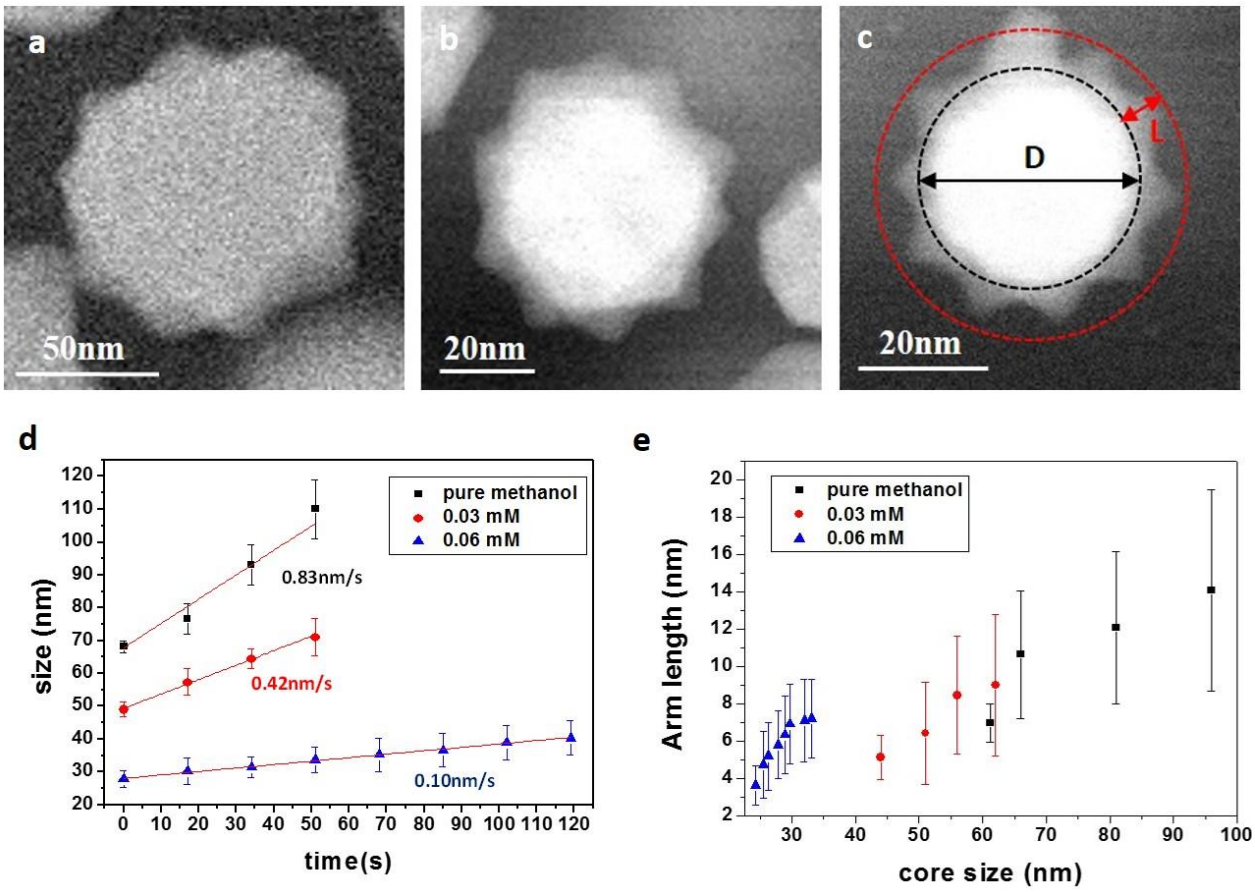

Figure 3. Effect of DMA on the growth mechanisms and final morphology of the Au NSs. *In situ* STEM-HAADF images showing the shape of NSs formed in the liquid-cell with a DMA concentration of **(a)** 0 mM (pure methanol), **(b)** 0.03 mM and **(c)** 0.06 mM. **(d)** Mean size of the NSs as the function of time for various DMA concentrations. The mean-growth speeds deduced from the linear fits of the data are indicated below each curve. **(e)** Averaged length of the NS arms (L) as a function of the averaged size of the NS core (D) for various DMA concentrations. An example of L and D measurements is shown in c. $\dot{d}$ = 3.4 electrons/Å^{2}s in all experiments.

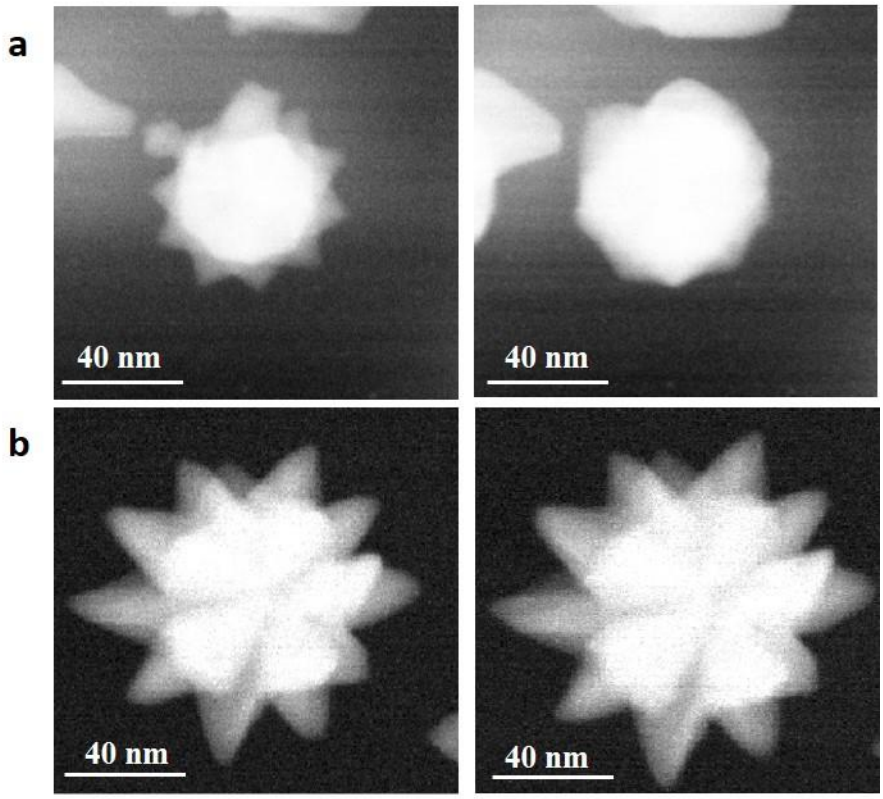

Figure 4. Stability of NSs as a function of DMA concentration. STEM-HAADF images acquired before (left images) and after (right images) a time (t) with no electron irradiation. **(a)** DMA concentration of 0.06 mM and t = 4 minutes. **(b)** DMA concentration of 0.2 mM and t = 7 minutes.

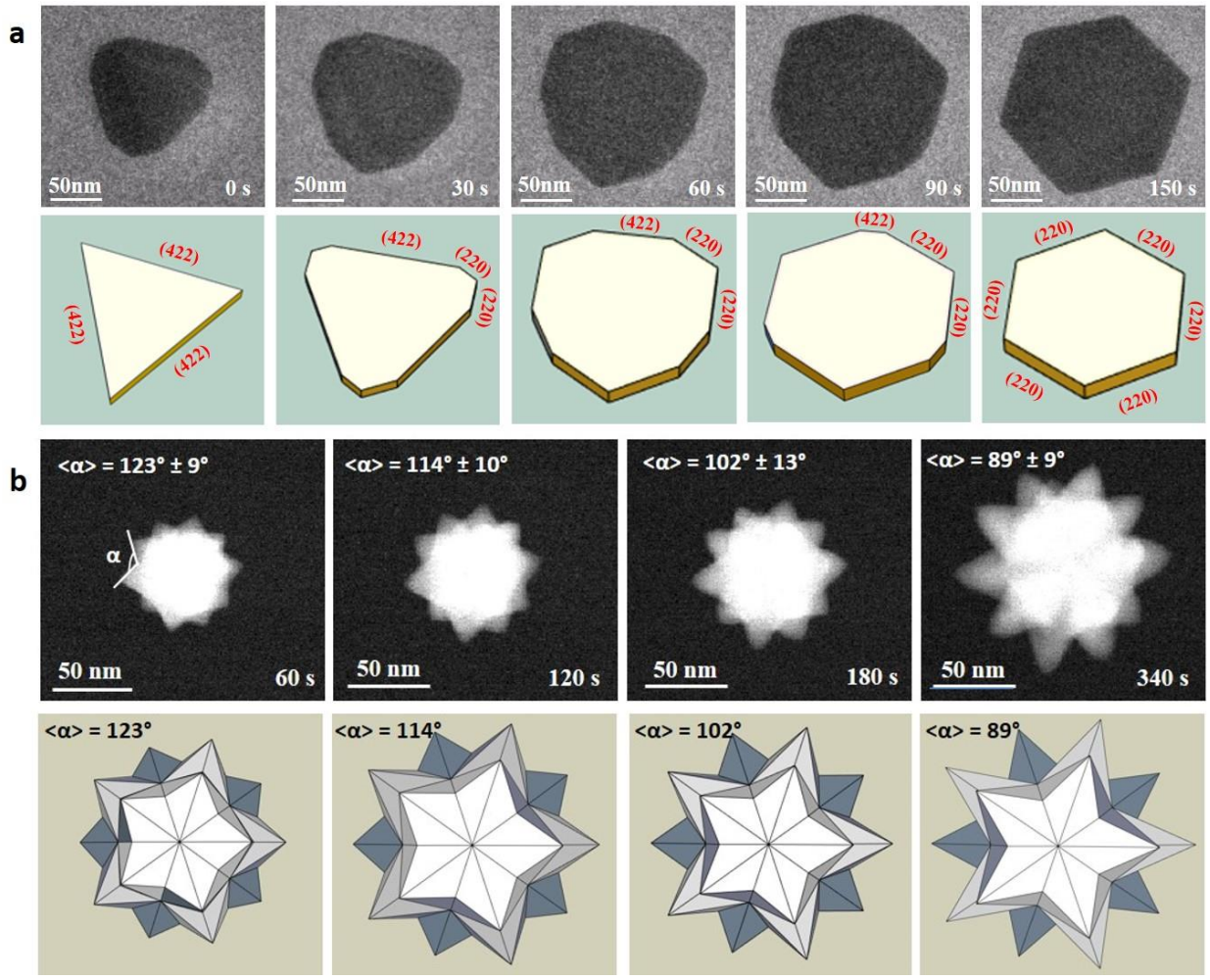

Figure 5. Growth mechanisms of Au nanostructures. (a) Time series of TEM images showing the transformation of a nanoprism into a hexagonal nanoplate in pure methanol. The irradiation time of the observed area is indicated in the bottom right corner of each image. The geometric models below the experimental images highlight the transformation process: the reshaping of the nanoprism corners creates six (220) edges that expand rapidly at the expense of the (422) edges because of the highest growth rate of the nanoprism along the [422] directions. See HRTEM images in Fig. S2c for the experimental indexation of the edges. **(b)** Time series of STEM-HAADF images showing the growth of a NS in methanol with a DMA concentration of 0.2 mM and $\dot{d}$ = 6 electrons/Å^{2}s. The irradiation time of the observed area and the means inter-arm angle (<α>) are indicated in the bottom right corner and the top left corners of each image, respectively. The geometric models below the experimental images highlight the transformation process: the growth rate of the 20 pyramidal arms is higher along the tip direction than along the basal plane leading to a sharpening of the arms and to a decrease of <α>.

Synopsis

Wet-chemical synthesis provides unique opportunities to fabricate complex metal nanostructures such as Au nanostars (NSs). Given the close link between the morphology and the technologically relevant properties of Au nanoparticles, it is imperative to understand the atomic-scale mechanisms leading to the formation of stellated nanostructures. In this letter, we exploit liquid cell transmission electron microscopy to reveal the growth mechanisms of symmetric NSs synthesized *via* a seed-mediated method in methanol. Besides revealing peculiar features of the stellation processes transforming icosahedral seeds into NSs with twenty sharp arms, this work provides valuable *in situ* insights to gain control over the shape of stellated Au nanoparticles in a simple alcohol solvent, which remains an important challenge to exploit the full potential of these nano-objects.

TOC Graphic